Journal of The Electrochemical Society

A Facile Segregation Process and Restoration of $LiMn_2O_4$ Cathode Material From Spent Lithium-Ion Batteries

Journal of The Electrochemical Society, 2020 **167** 090510

A Facile Segregation Process and Restoration of $LiMn_2O_4$ Cathode Material From Spent Lithium-Ion Batteries

Nithyadharseni Palaniyandy,[z] Khavharendwe Rambau, Nicholas Musyoka, and Jianwei Ren

Energy Materials, Energy Centre, Council for Scientific and Industrial Research (CSIR), Pretoria 0001, South Africa

Due to its three-dimensional tunnel structure, the spinel $LiMn_2O_4$ (LMO) cathode material is highly favourable for the migration of lithium ions. Thus, LMO has been used as a commercial cathode material for the electronic devices such as mobile phones and electric vehicles, owing to its special characteristics of low-cost, eco-friendly and non-toxic. However, the scarcity of lithium resources makes the system expensive. On the other hand, the tremendous and increasing usage of lithium ion batteries (LIBs) has undoubtedly generated a significant amount of spent LIBs, resulting in resource waste and environmental pollution. Therefore, in this work, we report on the recycling process of LMO from the spent LIBs and mainly devote to re-examine the electrochemical performances of the regenerated LMO cathode material, for the first time. It is noticed that, the renovated spinel LMO exhibits a better cycling stability up to 500 cycles, with the discharge capacity of 56 mAh g^{-1} and retained almost 100% of its initial capacity cycled at 1.0 C.

 [DOI: 10.1149/1945-7111/ab812d]

Manuscript submitted February 12, 2020; revised manuscript received March 17, 2020. Published April 2, 2020. *This paper is part of the JES Focus Issue on Battery Safety, Reliability and Mitigation.*

Due to the increasing demand of mobile phones, laptops and the electric vehicles, the production of lithium rechargeable batteries as a power source has exponentially increased. In this regard, the rapid growth of lithium-ion batteries requires a significant amount of metal resources, especially lithium (Li), cobalt (Co) and manganese (Mn).[1–8] Consequently, recycling of spent lithium-ion batteries has attracted significant attention in recent years due to the increasing demand for corresponding critical metals/materials and growing pressure on the environmental impact of solid waste disposal.[9–14]

Recently, LMO has been considered as a very popular cathode material for almost all commercialized lithium ion rechargeable batteries due to its high operating voltage, abundance, low manufacturing cost, low toxicity, and excellent voltage profile. Moreover, LMO has the advantage of fast charging because its delithiated spinel structure is relatively stable in terms of thermodynamics and structure compared to that of layered materials such as $LiCoO_2$, which in an overcharged state undergoes undesirable structural changes that degrade battery performance.[15–17] Therefore, it is anticipated that the recycling of spent LMO cathode material has numerous advantages such as an alternative Li resources, mitigation of environmental pollution, etc. In this study, we collected spent LIBs from mobile phones, carefully dismantle the batteries and used the resulting cathode materials for assembling new cells. The regenerated cathode materials were physically and electrochemically studied.

Experimental

Materials for preparation methods.—To renew the spinel LMO materials from spent LIBs, the collected spent LIBs were discharged using 2 M Na_2SO_4 for 24 h. Scissors were used to cut through the casing in order to detach the anode, cathode and the separator. The cathode material coated on the aluminium foil was immersed into the N-methyl-2-pyrrolidone (NMP) solution for a few hours before undergoing ultrasound sonication for 30 mins to separate the cathode material from the foil. The collected solution was also centrifuged for better separation. Since the obtained cathode material contains of LMO, PVDF and the electron-conducting carbon, the recovered materials were divided into two portions. One portion was heated at 700 °C for 2 h with a heating rate of 3 °C/min in order to remove the impurities such as binder and conductive carbon, while the other portion was only dried overnight at 100 °C for the comparison of their electrochemical performance. The schematic illustration of renovated spinel LMO process is shown in Fig. 1.

Materials characterisation techniques.—The structure and morphological characteristics of the renovated material was characterized by X-ray Diffraction (XRD), Scanning electron microscopy (SEM) and Transmission electron microscopy (TEM). XRD pattern was obtained using Rigaku Ultima IV powder X-ray Diffractometer with a monochromatized Cu Kα radiation of $\lambda = 1.5406$ Å at the 2θ range of 10°–80° and the lattice parameters derived by Rietveld refinement via TOPAS (3). SEM images were obtained using LEO 1525 field emission scanning microscope (FE-SEM) with the acceleration voltage of 2.00 kV. The TEM images were obtained using a JEOL HRJEM—2100 microscopy using LAB6 filament as an electron source. The chemical information of the resulting compounds was evaluated by X-ray photoelectron spectroscopy (XPS) using an AXIS ultra DLD spectrometer (KratosAnalytica) and a monochromatic Al $K\alpha$ excitation source (1486.6 eV) and the data was analysed by XPS peak 4.1 The binding energy (BE) scale was calibrated using a C 1s (BE = 284.6 eV) as the reference. X-ray fluorescence spectroscopy (XRF), following the fusion technique, was conducted using ARL ADVANT′X series in order to estimate the recovery of the LMO from the spent LIBs.

Electrochemical characterizations techniques.—The regenerated LMO electrode from spent LIBs was prepared for the re-utilization using 10% carbon black, 10% poly-vinylidene fluoride (PVDF) binder, and 80% active material (regenerated LMO). These materials were mixed using mortar and pestle in NMP solution. The prepared slurry was laminated on the Al foil using doctor blade method and dried overnight at 90 °C. The dried Al foil was cut into circular (12 mm) disc. The coin cells were fabricated in an argon filled glove box (MBraun), with the standard condition of O_2 and H_2O <0.5 ppm. The lithium foil, 1 M $LiPF_6$ in EC: DMC: DEC (1:1:1) volume ratio and the Cellgard 2300 polypropylene based membrane were used as anode, electrolyte, and separator, respectively.[18] The fabricated cells were evaluated using galvanostatic cycling performances, cyclic voltammetry (CV) and electrochemical impedance spectroscopy (EIS) by MACCOR series 4000 tester and a Bio-Logic VMP3 potentiostat/galvanostat, respectively.

[z]E-mail: nithyadharseni@gmail.com; NMusyoka@csir.co.za; NPalaniyandy@csir.co.za

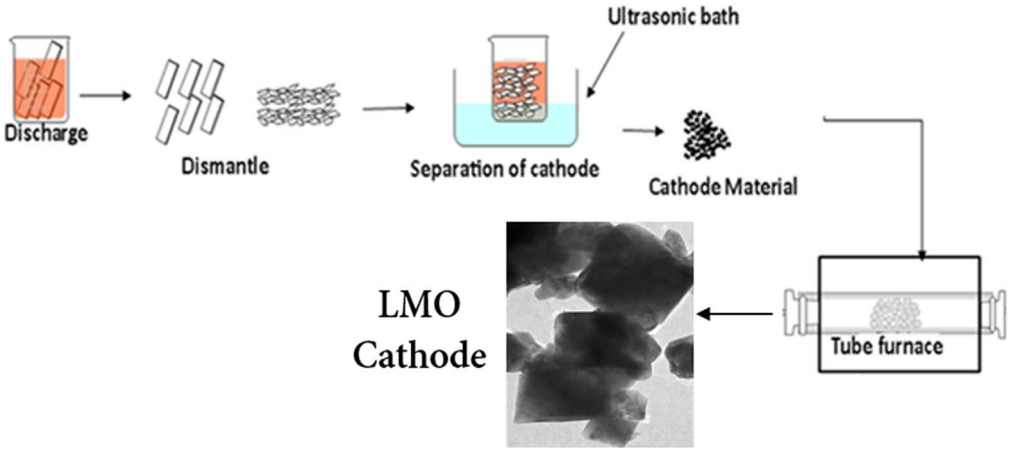

Figure 1. Schematic illustration of LMO cathode material synthesis process from spent LIBs.

Results and Discussion

The XRD patterns of restored LMO material from spend LIBs are illustrated in Figs. 2a–2d. The diffraction peaks of as-prepared and calcined at 700 °C samples can be indexed to spinel $LiMn_2O_4$ with the space group of Fd-3m, which remains the same as commercial LMO material after regenerated from spend LIBs. It was found that, the exact structural characterization of the prepared material is restrained with the normal peak intensities of pristine LMO.[19,20] However, the calcined LMO has few impurity peaks (marked with #) which belongs to Li_2MnO_3 that could be due to the further calcination process or possibly resulted from the insufficiencies of manganese and lithium during recycling process of LMO. These results match well with the reported literature as well as JCPDS pattern (#35-0782, a = b = c = 8.225 Å). Figure 2b shows no peak shift in the (111) diffraction peak, while other diffraction peaks exemplify in Figs. 2c, 2d. It was noted that there is slight peak shift

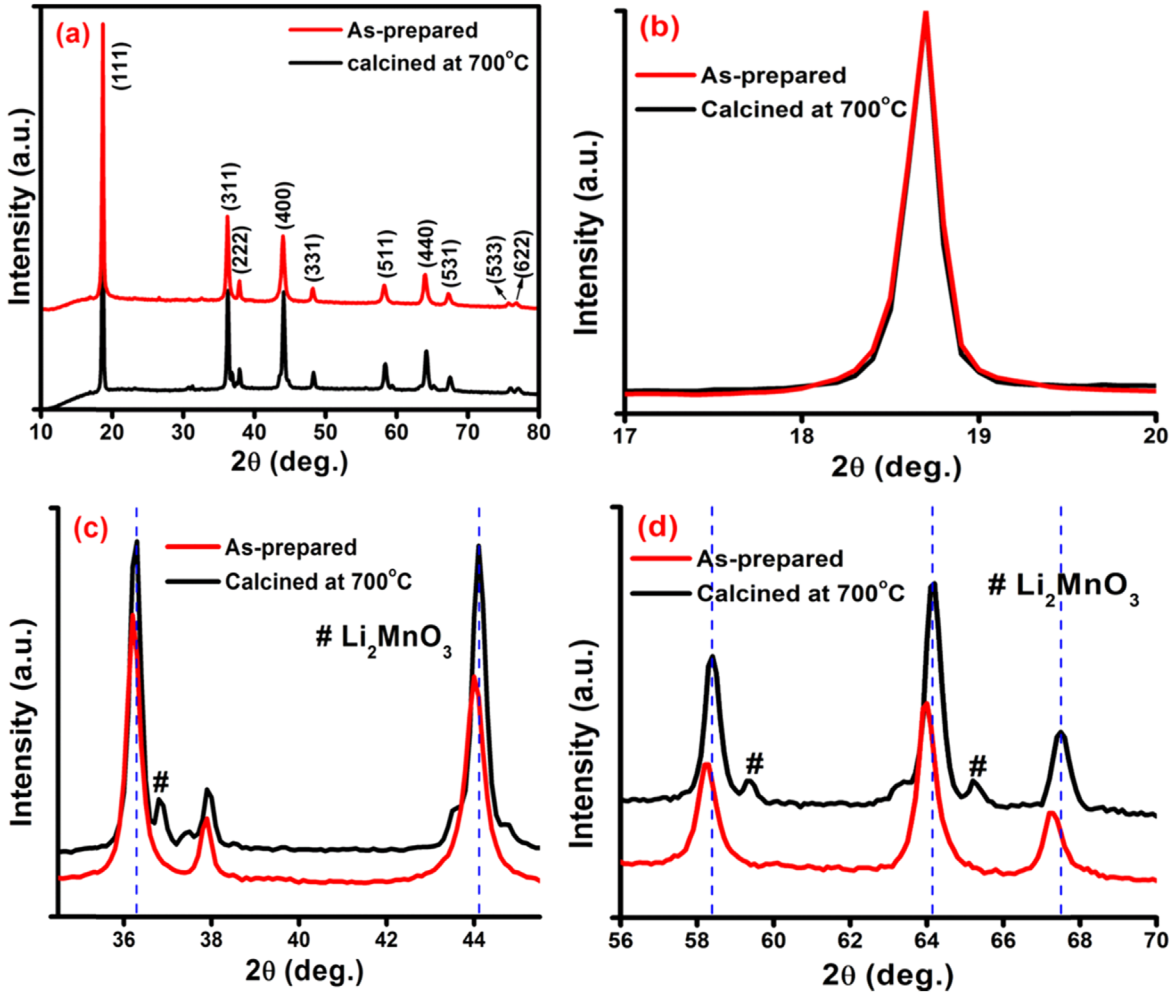

Figure 2. XRD patterns of as-prepared and calcined samples: (a) renovated LMO material, (b) enlarged XRD pattern from $2\theta = 17$ to 20 deg., (c) enlarged XRD pattern from $2\theta = 35$ to 45 deg. and (d) enlarged XRD pattern from $2\theta = 56$ to 70 deg.

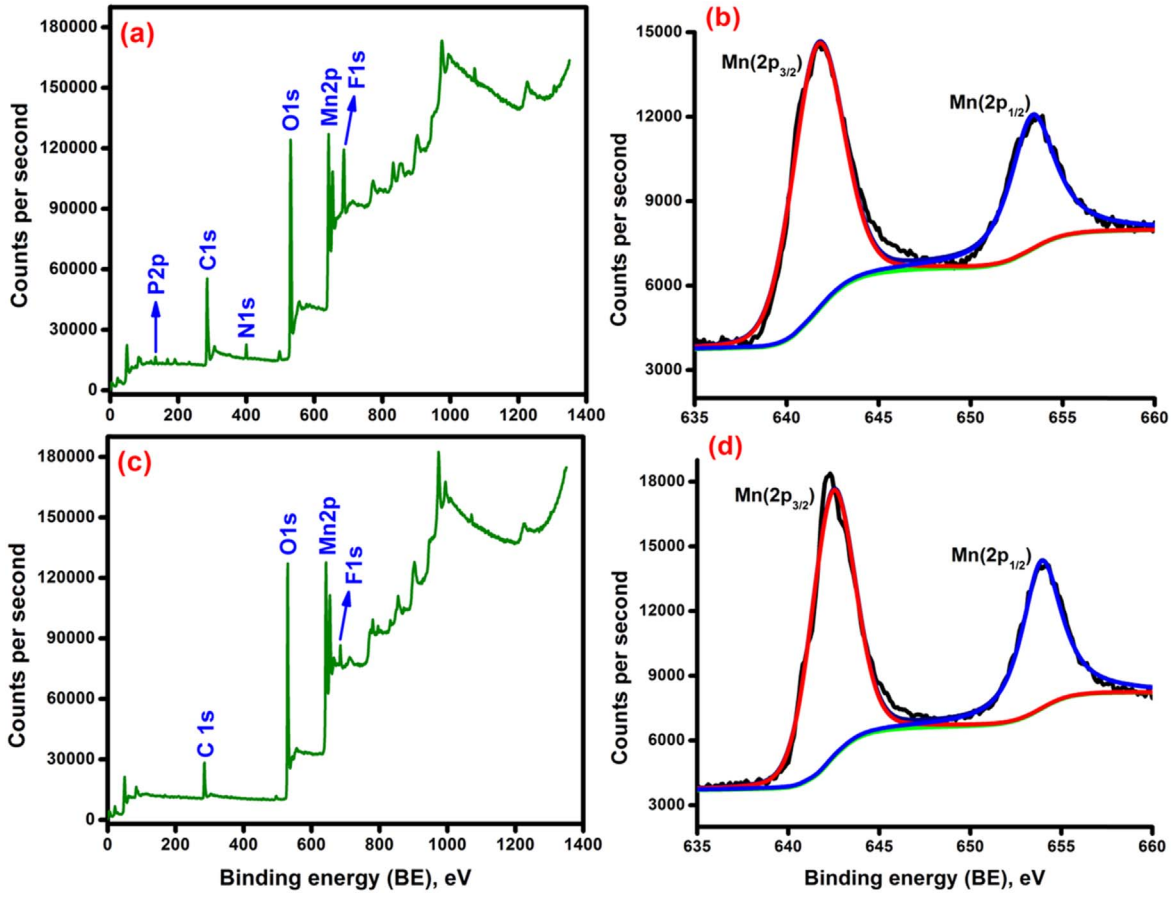

Figure 3. XPS spctrum of as-prepaerd and calcined regenerated LMO material: (a) and (c) full survey spectrum and (b) and (d) Mn 2p spectrum of as-prepaerd and calcined regenerated LMO material.

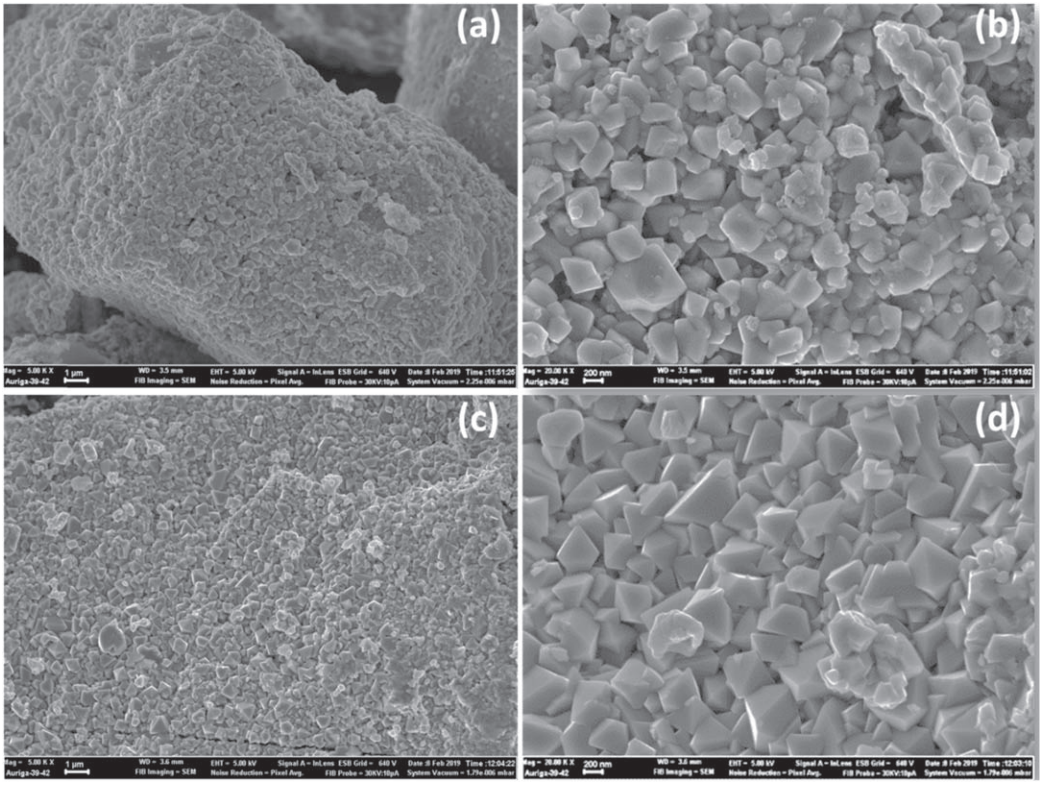

Figure 4. SEM images of regenerated LMO materials: (a), (b) low and high magnified as-prepared sample and (c), (d) low and high magnified calcined sample.

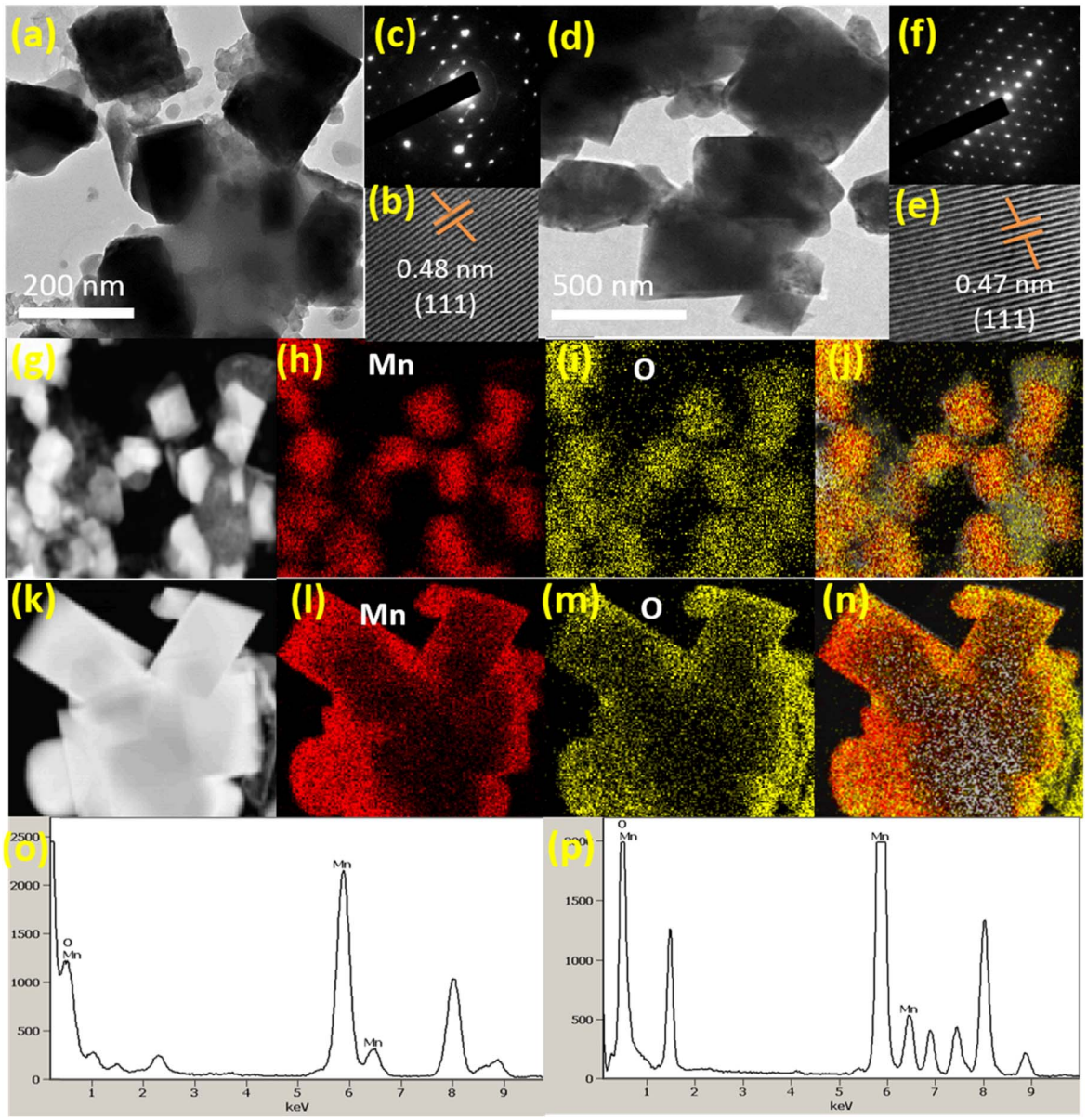

Figure 5. TEM images (a), (d) of regenerated LMO materials obtained from as-prepared sample and calcined cathodes together with corresponding HR-TEM images (b), (e), SAED pattern (c), (f). Elemental mapping images and EDX spectra of as-prepared LMO (g), (h), (i), (j) and (o) and calcined LMO (k), (l), (m), (n) and (p).

between the as-prepared and calcined samples, which is well evidenced due to the effect of the calcination process (Figs. 2c, 2d).[20–22] In addition, the slight peak shift is mainly instigated by the evolution of the lattice parameters. The lattice parameter and crystallite size was calculated using TOPAS; a = 8.229 Å, 52.5 nm for as-prepared sample and a = 8.202 Å, 67.2 nm for calcined sample.

The regenerated LMO from spent LIBs was further analysed using advanced XPS measurements to examine its chemical composition and surface chemical states. Figs. 3a and 3c is the full survey XPS spectrum of as-prepared and calcined LMO cathode. Fig. 3a implies the existence of P2p, C1s, N1s, O1s, Mn2p and F1s elements in the as-prepared sample, while the calcined sample (Fig. 3b) displays C1s, O1s, Mn2p and F1s elements. It is clearly understandable that the calcination process completely eliminates the N and P elements in the calcined sample. The Mn2p spectrum of as-prepared sample exhibits one doublet peak at 641.8 V and 653.4 eV, while the calcined sample shows two peaks at 642.6 and 654 eV, corresponding to Mn $2p_{3/2}$ and Mn $2p_{1/2}$. The spin-energy separation of as-prepared and calcined samples are 11.6 and 11.4 eV and these values are in very good agreement with reported literature data, indicating 4^{+} oxidation states of Mn.[22–26] Also, the obtained fluorine content in both samples, may be from the PVDF or electrolyte solution, however, the intensity of fluorine peak was decreased in the calcined sample. This results indicates that the regenerated LMO from spent LIBs is pure phase of LMO with minor impurities of F, N and P.

The morphologies of renovated LMO were examined using SEM, and the images of as-prepared and calcined samples are shown in Figs. 4a–4d. SEM morphologies of as-prepared and calcined samples consist of crystalline particles with hexagonal shape.[19,20] The as-prepared sample demonstrates crystalline nature and agglomerated grains consists of sub-micron sized particles, while, the calcined sample exhibits well-crystalline nature and sub-micron sized particles with uniformed morphology.[19] However, in both samples, the primary particles are sub-micros within the range of 100–300 nm. It is noted that the morphologies of the regenerated

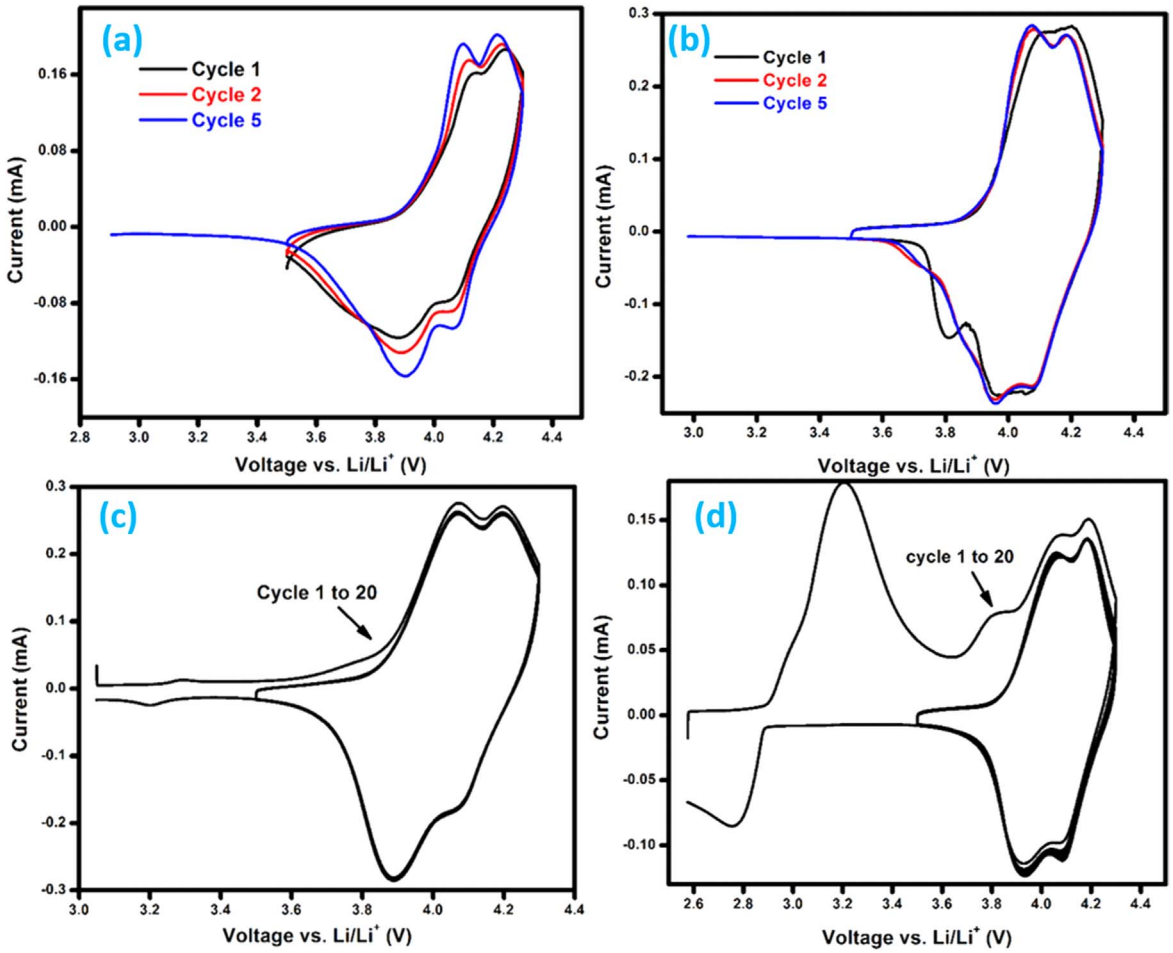

Figure 6. CV analysis of regenerated LMO: (a) As-prepared LMO and (b) calcined LMO before cycling (at open circuit voltage). (c) As-prepared LMO and (d) calcined LMO after 500 cycles at 0.1 C, with the potential window between 3.5 to 4.3 V for all CV spectra.

LMO is well-matched with literatures and commercial LMO. We strongly believe that the renovation mechanism process does not affect the primary morphology of the LMO cathode materials.

To further investigate the microstructure, size and chemical compounds of the as-prepared and calcined LMO materials, TEM analysis was carried out and the results presented in Figs. 5a–5p. TEM micrographs of as-prepared and calcined LMO particles (Figs. 5a, 5d) are in the sub-micron range, however, the obtained calcined particles are bigger when compared to the as-prepared sample. The HR-TEM images of both as-prepared and calcined LMO cathodes (Figs. 5b, 5e) show the lattice fringe d-spacing of ~0.47 nm which corresponds to the (111) plane.[27] The selected area diffraction (SAED) pattern (Figs. 5c, 5f) demonstrates the crystalline nature of the LMO cathodes. In addition, the mapping images of as-prepared (Figs. 5g–5j) and calcined (Figs. 5k–5n) LMO exhibits that both Mn and O are distributed uniformly and EDX pattern shows the presence of these elements. According to the XRF report, we roughly calculated that around 97.535% of LMO was retrieved during recycling process and other impurities of F (0.069), P (0.057), N (0.028), Al_2O_3 (0.217), SiO_2 (0.027), Na_2O (0.593), TiO_2 (0.013), SO_3 (1.123), CaO (0.050), MgO (0.221), K_2O (0.053), BaO (0.014) were around 2.465%, since the lithium cannot be analysed by using XRF analysis. Therefore it is suggested that there is a need for further analysis to discover the exact amount of recycled LMO.

To re-evaluate the electrochemical performance of restored LMO prepared from spent LIBs, CV analysis was carried out in the potential range of 3.5 to 4.3 V, at the scan rate of 0.1 mV s^{-1}. It can be seen that, all the CV curves of LMO materials (Figs. 6a–6d) displays two pairs of redox peaks at 3.9/4.1 V and 4.05/4.2 V, corresponding to two-step lithium insertion/extraction process in to the tetrahedral sites.[16,28,29] To further evaluate the electrochemical performance of restored LMO prepared from spent LIBs, the samples were galvanostatically tested at two different potential ranges, at 3.5−4.3 V and 3.5−4.9 V, in order to evaluate the stability of the electrodes, as shown in Figs. 7 and 8.

The fabricated half-cell was galvanostatically cycled at a current density of 0.1 C (14.8 mAh g^{-1}) and 1 C (148 mAh g^{-1}). Figs. 7a, 7b depicts the corresponding first few charge and discharge cycles of LMO materials, cycled between the voltage window of 3.5 to 4.9 V. Both samples exhibits two redox curves around at 3.9/4.1 V and 4.0/4.2 V, indicating an expected two-step lithium ion insertion/extraction reactions.[28,29] The observed first cycle charge/discharge capacities of as-prepared and calcined samples are 167/88 mAh g^{-1} and 147/83 mAh g^{-1} cycled between 3.5 to 4.9 V. Fig. 7c demonstrates the cycling performance of LMO materials, as-prepared LMO shows higher capacity in the initial cycle (166 mAh g^{-1}) than that of calcined LMO (124 mAh g^{-1}), however, rapid capacity fading was observed.[29–31] Nevertheless, calcined LMO illustrates gradual capacity fading up to 300 cycles. The rapid capacity fade during the initial cycles of both samples could be attributed to the lack of lithium during insertion/de-insertion process when the LMO charged at high voltage at 4.9 V, (cut-off potential 3.5 to 4.9 V). Overall, the specific capacity of 80 mAh g^{-1} (at 239th cycle) and 71 mAh g^{-1} (at 298th cycle) was obtained with the capacity retention of 60% and 63% for as-prepared and calcined LMO cathode at the end of the 500 cycles, respectively.

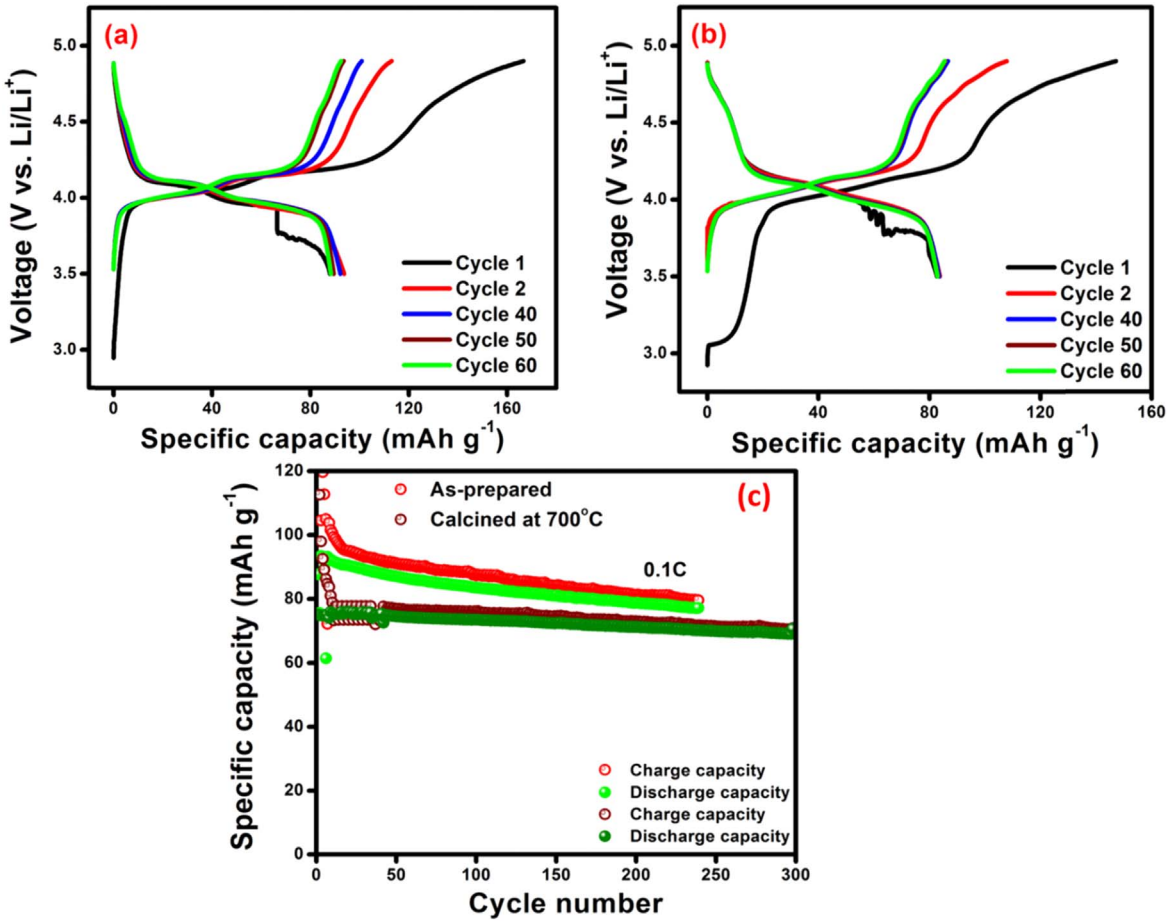

Figure 7. Galvanostatic cycling of renovated LMO matereials: (a) as-prepared, (b) calcined at 700 °C, and (c) cyclic performance of LMO material cycled at 0.1 C with the potential window 3.5–4.9 V.

Figs. 8a, 8b represents the corresponding first few charge/discharge cycles (1, 2, 10, 30 and 50) of LMO materials, cycled at 3.5 to 4.3 V. In the charge/discharge spectrum, the samples exhibits two redox curves around at 3.9/4.1 V and 4.0/4.2 V, indicating an expected two-step lithium ion insertion/extraction reactions which is in good agreement with CV analysis (Fig. 6).[28,29] The acquired first charge/discharge capacities of LMO cathode materials are 125/66 mAh g^{-1} and 105/46 mAh g^{-1} when cycled at 0.1 C whereas at 1.0 C the capacities are 88/47 mAh g^{-1} and 67/54 mAh g^{-1} for the as-prepared and calcined samples, respectively. At 0.1 C, calcined cathode material demonstrated lower capacity, compared to its counterpart, however, capacity is maintained stable, which is evident with the Fig. 8b, after 10th cycle where the discharge/charge characteristics are overlapped, unlike as-prepared cathode material (Fig. 8a). The capacity variation for the first 10 cycles for both samples, could be due to the structural changes during lithium insertion/de-insertion process. The discharge capacities of 59 mAh g^{-1} and 54 mAh g^{-1}, with the capacity retention of 63.4% and 53% at the end of the 500th cycles for as-prepared and calcined materials were obtained, respectively. Higher capacity was found for as-prepared cathode, however, both LMO (Fig. 8c) demonstrates an obviously lower fading rate upon cycling which reveals the good reversibility during the Li^+ ion intercalation/deintercalation process. Nevertheless, when cycled at 1.0 C, high capacity of 56 mAh g^{-1} was observed for calcined LMO than that of its counterpart (45 mAh g^{-1}), while the capacity retention of 95% and 90% was revealed for calcined and as-prepared LMO cathodes at the end of the 500th cycles. In both materials, almost 100% columbic efficiency was observed.

To further report the electrochemistry performances of the cathodes, EIS analysis was carried out on before and after cycling of the LMO cathodes (Figs. 9a, 9b). The Nyquist plots were fitted using an electrical equivalent circuit as shown in inset image of Fig. 9a. The obtained R_s value for as-prepared sample is 17 (±1) Ω and 130 (±1) Ω, while 2 (±1) Ω and 14 (±1) Ω is observed for calcined sample at after and before cycling, respectively. The charge transfer (Rct) resistances are 563, 131 (±5) Ω and 439, 95 (±5) Ω, respectively at open circuit voltage (OCV) and after cycling for as-prepared and calcined materials. It can be seen that the electrolyte resistance of the as-prepared sample is higher than the calcined sample measured at OCV, while EIS measured after cycling exhibited negligible electrolyte resistance in both LMO cathodes. It clearly demonstrates that the calcined LMO cathode exhibits low charge-transfer resistance compared to the as-prepared LMO cathode, leading to an enhanced electrochemistry performance (improved capacity and capacity retention) which is in good agreement with Fig. 8d. In addition, the low frequency region (Warburg region) of both samples reveal linear shape and the slope of each line characterizes better Li ion diffusion kinetics behaviour during intercalation/de-intercalation process.[16,29]

Conclusions

Renovated spinel $LiMn_2O_4$ cathode material was prepared from spent LIBs following a two-step chemical process and re-examined for its electrochemical properties for LIBs. The chemical procedure/technology we applied in this work can be expected to serve as an effective or easy route for the recycling of spent lithium rechargeable batteries. However, from the XRF analysis it was found that the separation of LMO from the above procedure is not completely

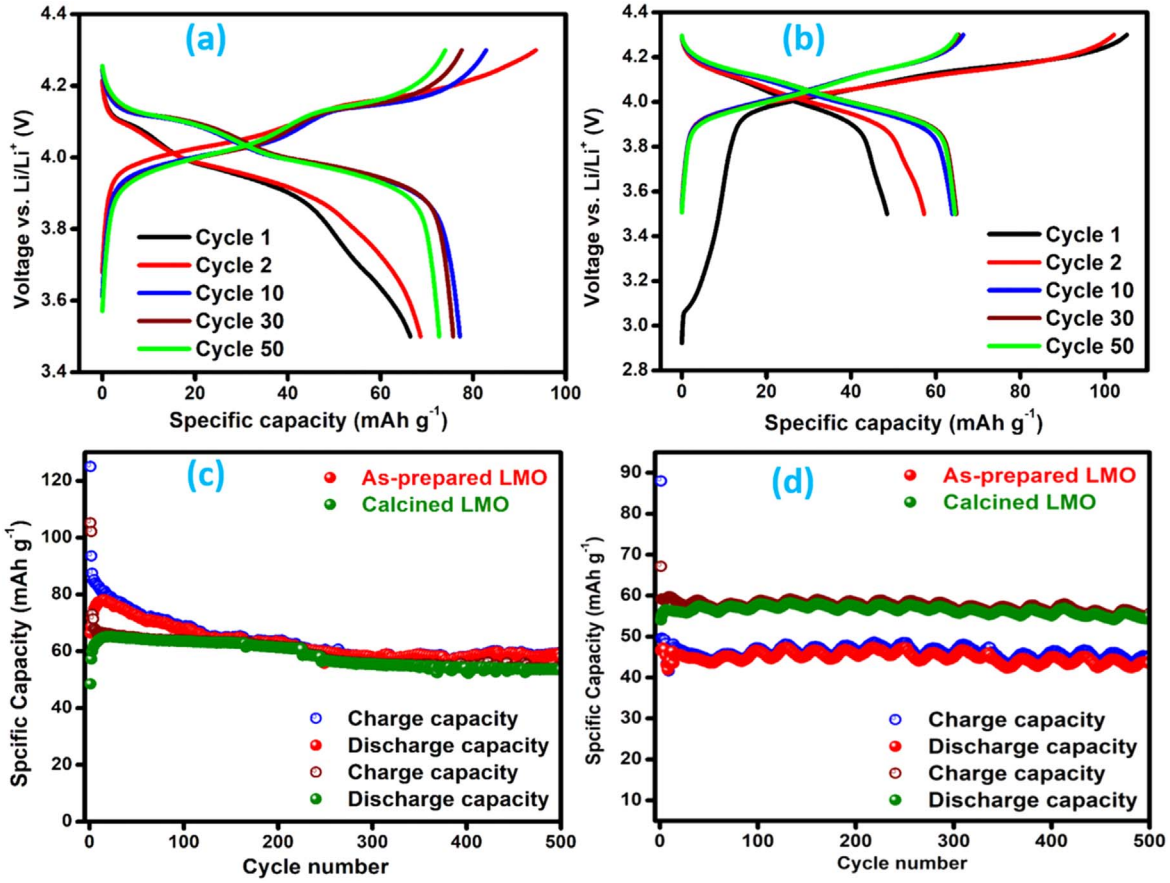

Figure 8. Galvanostatic cycling of (a) as-prepared and (b) calcined LMO at first few charge/discharge cycles. Cycling performance (c) at 0.1 C and (d) at 1.0 C of LMO materials with the potential window of 3.5–4.3 V.

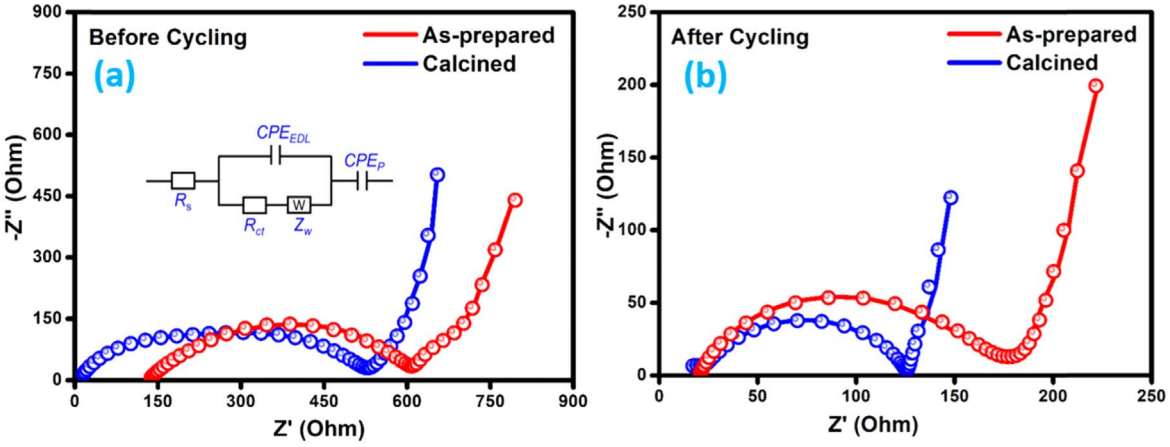

Figure 9. Comparative Nyquist plots of as-prepared and calcined LMO materials measured (a) before with the fitted equivalent circuit and (b) after cycling.

achieved. Nonetheless, the physical and chemical characterizations show the renovated LMO phase to be an encouraging cathode material for lithium rechargeable batteries. However, the prepared LMO phase shows some impurities such as P, F and N as confirmed from XPS analysis and electrochemistry analysis which showed low capacity. Therefore, it is anticipated that with further purification or used of a different chemical synthesis process pure phase materials can be obtained. According to literature, we suggested that, the direct (after dismantle the cathode materials from spent LIBs) hydrothermal reaction would be able to separate and accumulate the electrochemically reactive species which will have a much better performance. Therefore, our next approach/aim is to adopt hydrothermal technique to synthesis phase pure LMO/LCO cathode material from spent LIBs.

Acknowledgments

The authors would like to thank the Council for Scientific and Industrial Research (CSIR) for providing the funding (project number EIMH10P) to make this study possible.

ORCID

Nithyadharseni Palaniyandy https://orcid.org/0000-0001-8960-6735

References

1. W. Lv, Z. Wang, H. Cao, Y. Sun, Y. Zhang, and Z. Sun, *ACS Sustainable Chem. Eng.*, **6**, 1521 (2018).
2. J. Hu, J. Zhang, H. Li, Y. Chen, and C. Wang, *J. Power Sources*, **351**, 199 (2017).
3. D. S. Kim, J. S. Sohn, C. K. Lee, J. H. Lee, K. S. Han, and Y. I. Lee, *J. Power Sources*, **132**, 149 (2004).
4. R. Golmohammadzadeh, F. Rashchi, and E. Vahidi, *Waste Manage. (Oxford)*, **64**, 254 (2017).
5. J. Xiao, J. Li, and Z. Xu, *J. Hazard. Mater.*, **338**, 131 (2017).
6. X. Zheng, W. Gao, X. Zhang, M. He, X. Lin, H. Cao, Y. Zhang, and Z. Sun, *Waste Manage. (Oxford)*, **60**, 688 (2017).
7. X. Chen, H. Ma, C. Luo, and T. Zhou, *J. Hazard. Mater.*, **326**, 86 (2017).
8. J. Ordonez, E. J. Gago, and A. Girard, *Renew. Sust. Energ. Rev.*, **60**, 205 (2016).
9. H. Ku, Y. Jung, M. Jo, S. Park, S. Kim, D. Yang, K. Rhee, E. M. An, J. Sohn, and K. Kwon, *J. Hazard. Mater.*, **313**, 146 (2016).
10. L. P. He, S. Y. Sun, X. F. Song, and J. G. Yu, *Waste Manage. (Oxford)*, **64**, 181 (2017).
11. Y. Yang, S. Xu, and Y. He, *Waste Manage. (Oxford)*, **64**, 227 (2017).
12. X. Zheng, Z. Zhu, X. Lin, Y. Zhang, Y. He, H. Cao, and Z. Sun, *Engineering*, **4**, 370 (2018).
13. J. Yu, Y. He, Z. Ge, H. Li, W. Xie, and S. Wang, *Sep. Purif. Technol.*, **190**, 52 (2018).
14. E. G. Pinna, M. C. Ruiz, M. W. Ojeda, and M. H. Rodriguez, *Hydrometallurgy*, **167**, 71 (2017).
15. F. P. Nkosi, C. J. Jafta, M. Kebede, L. L. Roux, M. K. Mathe, and K. I. Ozoemena, *RSC Adv.*, **5**, 32256 (2015).
16. W. Huang et al., *Nano Energy*, **64**, 103936 (2019).
17. M. A. Kebede, N. Palaniyandy, and L. F. Koao, *Electrochemical Devices for Energy Storage Applications*, **1**, 17 (2019).
18. F. P. Nkosi, N. Palaniyandy, K. Raju, K. Billing, and K. I. Ozoemena, *Mater. Res. Express*, **6**, 115501 (2019).
19. P. R. Ilango, K. Prasanna, S. J. Do, Y. N. Jo, and C. W. Lee, *Sci. Rep.*, **6**, 29826 (2016).
20. E. Hu, S. M. Bak, S. D. Senanayake, X. Q. Yang, K. W. Nam, L. Zhang, and M. Shao, *J. Power Sources*, **277**, 193 (2015).
21. H. Wang, K. Huang, Y. Zhang, X. Chen, W. Jin, S. Zheng, and P. Li, *ACS Sustainable Chem. Eng.*, **5**, 11489 (2017).
22. L. Li, R. Chen, F. Sun, F. Wu, and J. Liu, *Hydrometallurgy*, **108**, 220 (2011).
23. L. E. Sita, S. P. Silva, P. R. C. Silva, and J. Scarminio, *Mater. Chem. Phy.*, **194**, 97 (2017).
24. P. Liu, L. Xiao, Y. Tang, Y. Zhu, H. Chen, and Y. Chen, *Vacuum*, **156**, 317 (2018).
25. N. Palaniyandy, F. P. Nksoi, K. Raju, and K. I. Ozoemena, *Mater. Chem. Phy.*, **209**, 75 (2018).
26. M. Lu, H. Zhang, B. Wang, X. Zheng, and C. Dai, *Int. J. Electrochem. Sci.*, **8**, 8201 (2013).
27. L. Li, R. Chen, X. X. Zhang, F. Wu, J. Ge, and M. Xie, *Chinese Sci. Bull.*, **57**, 4188 (2012).
28. H. Dong and G. M. Koenig, *Cryst. Eng. Comm.*, **22**, 1514 (2020).
29. L. Li, E. Fan, Y. Guan, X. Zhang, Q. Xue, L. Wei, F. Wu, and R. Chen, *ACS Sustainable Chem. Eng.*, **5**, 5224 (2017).
30. T. Or, S. W. D. Gourley, K. Kaliyappan, A. Yu, and Z. Chen, *Carbon Energy*, **1**, 38 (2020).
31. C. Zhenfei et al., *J. Energy Storage*, **27**, 101036 (2020).